Multiscale Surface Patterning of Zirconia by Picosecond Pulsed Laser Irradiation

Yuka Yamamuro
Department of Mechanical Engineering,
Faculty of Science and Technology,
Keio University,
Hiyoshi 3-14-1,
Kohoku-ku, Yokohama 223-8522, Japan

Tomotaka Shimoyama
Advanced Materials Research Laboratory,
TOSOH Corporation,
Hayakawa 2743-1,
Ayase 252-1123, Japan

Isao Yamashita
Advanced Materials Research Laboratory,
TOSOH Corporation,
Hayakawa 2743-1,
Ayase 252-1123, Japan

Jiwang Yan[1]
Department of Mechanical Engineering,
Faculty of Science and Technology,
Keio University,
Hiyoshi 3-14-1,
Kohoku-ku, Yokohama 223-8522, Japan
e-mail: yan@mech.keio.ac.jp

Irradiation of yttria-stabilized zirconia (YSZ) was performed by a picosecond pulsed laser to investigate the possibility for multiscale surface patterning. Nanoscale laser-induced periodic surface structures (LIPSS) were successfully generated inside microscale grooves over a large surface area under specific conditions. A thermally induced phase transformation of YSZ was identified after laser irradiation, and this phase transformation was restrained by reducing the laser power or the number of irradiations. Moreover, it was found that the generation of LIPSS greatly changed the surface wettability of YSZ. These results demonstrated the possibility of creating zirconia hybrid patterns with high functionality, which may expand the applications of YSZ in industry. [DOI: 10.1115/1.4046040]

Keywords: zirconia, nanostructure, ultrashort pulses, surface patterning, phase transformation, surface wettability

1 Introduction

Yttria-stabilized zirconia (YSZ) is a fine ceramic material which has high strength and wear resistance [1,2]. In recent years, the demand of YSZ is increasing in various fields. Especially, it is used as an alternative to conventional metallic materials in many applications such as dental implants, electronic substrates and optical fiber connectors [3–5].

For surface functionalization and performance enhancement, such as biocompatibility improvement of medical devices, as well as device miniaturization, micro/nanoscale surface patterning for YSZ is needed. However, since YSZ is hard, brittle and chemically stable, it is difficult to process YSZ by mechanical and chemical methods [6]. Especially, it is difficult to achieve high precision in the micro/nanoscale. To solve these issues, laser irradiation has been used as an effective microfabrication method in recent years. As laser irradiation is a noncontact process, there is no problem of tool wear and breakage. Moreover, laser irradiation enables machining complex shapes over a large surface area in a short time.

However, it was reported that the heat affected zone led to strength degradation of YSZ when a nanosecond pulsed laser was used [4,5,7]. Therefore, laser ablation by ultrashort pulsed laser might be effective because an ultrashort pulse can minimize the thermal effect. The ablation process can be finished before the thermal diffusion around the irradiated area. In addition, Bashir et al. found that periodic nanostructures, i.e., laser-induced periodic surface structures (LIPSS), were formed on the surface of YSZ by using femtosecond pulsed laser irradiation [8]. In recent years, many other researchers are also focusing on femtosecond laser irradiation for LIPSS generation on zirconia surface [9,10]. However, up to date, there are few researches on picosecond pulsed laser processing of YSZ, and thus its laser processing characteristics are unclear [11].

In this study, we propose a multiscale surface patterning method of YSZ by laser processing using picosecond pulses. We investigated the fundamental characteristics of microgrooving and nanoscale LIPSS formation inside the grooves. Furthermore, we evaluated the laser induced phase transformation of YSZ material, and explored the conditions for suppressing it.

2 Experiment

The laser used in following experiments was PFLA-1030TP, an Yb fiber laser made by Optoquest Co., Ltd., Japan. The laser wavelength was 1030 nm and the repetition frequency was 100 kHz. The energy density of the laser beam had a Gaussian distribution. The laser spot was an ellipse with a size of 6 μm × 7 μm and the focal length was 20 mm. The workpiece movement was driven by a stage in X, Y, and Z directions. The laser beam was focused on the workpiece surface by using a CCD camera which had the same focal length as the laser. As a workpiece, ZrO_2 containing 3 mol % Y_2O_3 for stabilization made by Tosoh Co., Ltd, was used. The sample dimensions were $23 \times 23 \times 5\,mm^3$ and the surface was mirror-polished after sintering. The experimental conditions are shown in Table 1, and the irradiation schemes in Fig. 1. Line irradiation and plane irradiation were performed, respectively, by controlling the movement of the sample stage.

After laser irradiations, the surface morphologies of the samples were observed by a scanning electron microscope (SEM), Inspect F50, made by FEI Company, U.S. The depth of irradiated area was measured by a laser microscope, OLS4100, made by Olympus Corporation, Japan. The profile of the surface nanostructure was observed by an atomic force microscope (AFM), SPM-3, made by Hitachi High-Technologies Corporation, Japan. Phase transformation was evaluated by a laser micro-Raman

Table 1 Experimental conditions

Laser medium	Yb
Wavelength (nm)	1030
Spot size (μm)	Ellipse (major axis 7, minor axis 6)
Pulse width (ps)	50, 240
Repetition frequency (kHz)	100
Scanning speed (mm/s)	1.0, 5.0, 10
Laser fluence: f (J/cm^2)	3.0–7.0
Number of irradiations: N	1–10
Scanning pitch (μm)	2.0

[1]Corresponding author.

Contributed by the Manufacturing Engineering Division of ASME for publication in the Journal of Micro- and Nano-Manufacturing. Manuscript received October 31, 2019; final manuscript received December 20, 2019; published online February 13, 2020. Assoc. Editor: Lawrence Kulinsky.

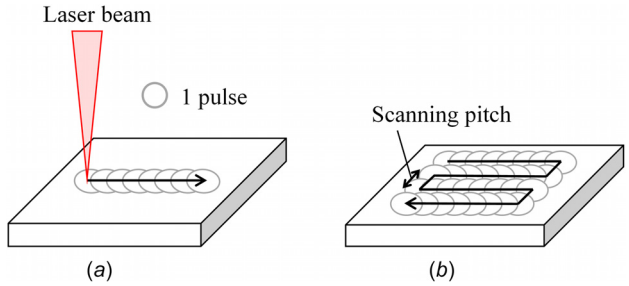

Fig. 1 Irradiation schemes: (*a*) line irradiation and (*b*) plane irradiation

spectrometer, NRS-3100, made by JASCO Co., Ltd., Japan. To evaluate the surface wettability, the contact angle of the surface was calculated by a contact angle meter, Simage Entry 5, made by Excimer, Inc., Japan.

3 Results and Discussion

3.1 Effect of Laser Fluence. Line irradiation was performed at a scanning speed of 5.0 mm/s and the laser was scanned only once. The SEM images of YSZ surface irradiated at different fluence are shown in Fig. 2 (pulse width: 50 ps). When $f = 3.0$ J/cm^2, the irradiated mark is very shallow; when $f = 7.0$ J/cm^2, a deep groove was generated with pileups on two sides. The changes of groove depth with laser fluence for two different pulse widths (50, 240 ps) are shown in Fig. 3. The groove depth increases logarithmically with fluence, which is similar to the trends in nanosecond pulsed laser irradiation [4,12]. This is because as the laser fluence increases, the absorption of laser by the material also increases, which results in an increase in material removal rate. Moreover, at a constant laser fluence, as the pulse width becomes shorter, the peak power per pulse increases, then the groove depth can be deeper.

3.2 Effect of Number of Irradiations. Line irradiation was performed at a pulse width of 50 ps, a laser fluence of 7.0 J/cm^2 and scanning speed of 1.0 mm/s with different number of irradiations. The SEM images of the irradiated surface at each irradiation number are shown in Fig. 4. When $N = 5$, a smooth surface was observed at the groove bottom (Fig. 4(*a*)). On the other hand, when $N = 10$, LIPSS were formed on the bottom and sides of the groove (Fig. 4(*b*)). The period of LIPSS was about 300 nm, distinctly shorter than the laser wavelength (1030 nm). The groove

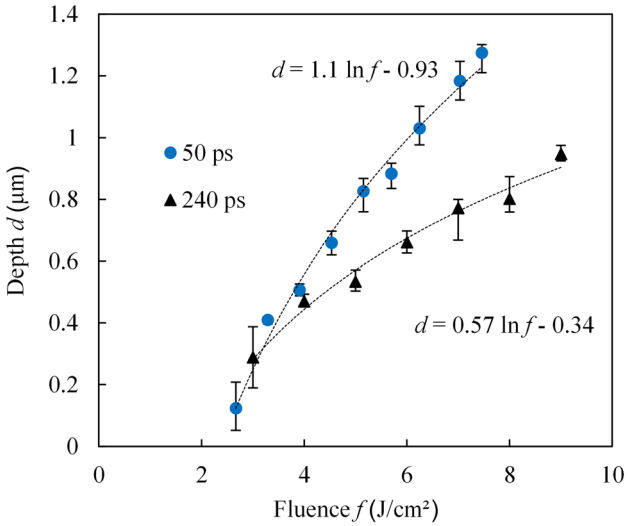

Fig. 3 Change in groove depth with fluence

depth versus the number of irradiations and laser fluence at the bottom of the groove are plotted in Fig. 5. The laser fluence f was calculated from the result of groove depth at each number of irradiations. Since the laser beam had a Gaussian distribution, the laser spot diameter $\omega(x)$ at a defocused position x, corresponding to groove depth, was calculated by the following equation:

$$\omega^2(x) = \omega_0^2\left[1 + \left(\frac{\lambda x}{\pi\omega_0^2}\right)^2\right] \tag{1}$$

where ω_0 is the spot diameter at the focal position, and λ is laser wavelength. Subsequently, the laser fluence f at the bottom of the groove was calculated by using the spot diameter $\omega(x)$ and the following equation:

$$f = \frac{4E}{\pi\omega^2(x)} \tag{2}$$

where E is the average laser power of one pulse. As shown in Fig. 5, the laser fluence was decreased with the number of irradiations. It is presumable that the repeated irradiation caused an increase in the groove depth which, in turn, caused the LIPSS formation. In general, LIPSS only form when the laser fluence is near the ablation threshold [8,13]. At the bottom of the groove,

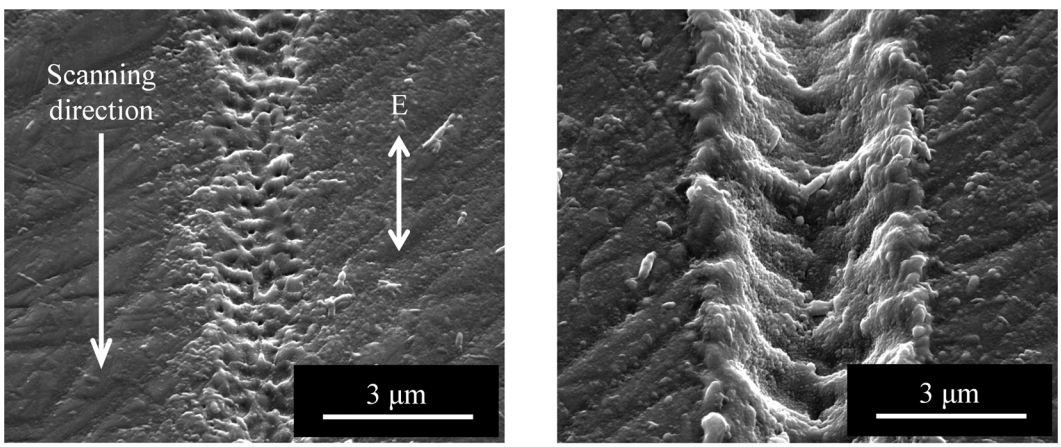

Fig. 2 SEM images of surface irradiated with 50 ps pulses at various fluence: (*a*) 3.0 J/cm^2 and (*b*) 7.0 J/cm^2

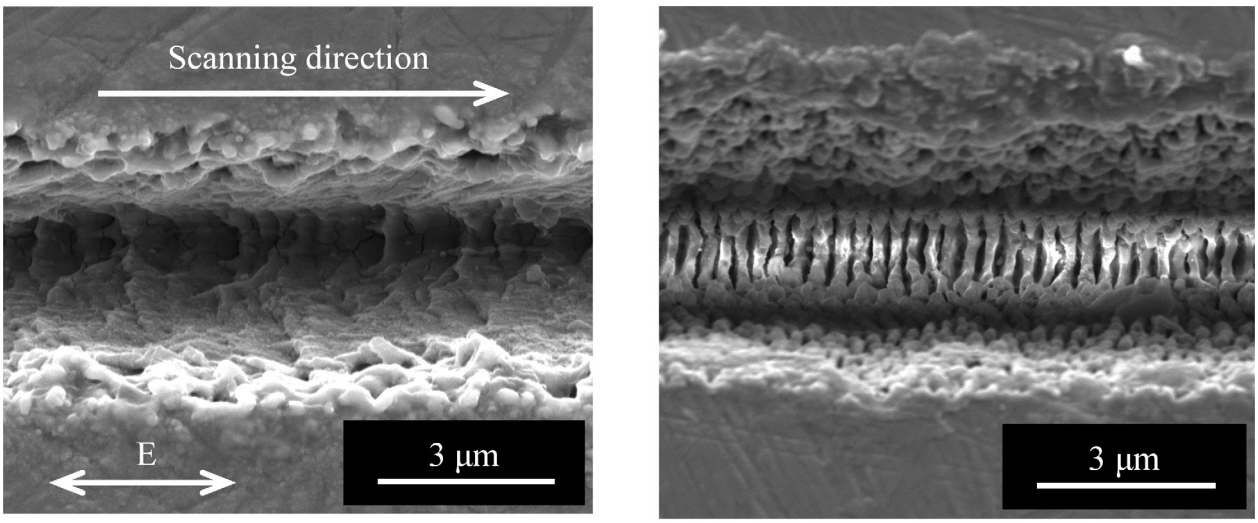

Fig. 4 SEM images of surface formed after various number of irradiations: (*a*) $N = 5$ and (*b*) $N = 10$

laser fluence decreases due to the defocus of the laser beam. When $N = 5$, the groove was shallow, thus defocus was small, and the laser fluence was too high to form LIPSS. However, when $N = 10$, the depth of the groove (the defocus amount) increased and the laser fluence at the groove bottom decreased sufficiently, thus the LIPSS formed. Furthermore, LIPSS formation might also have been affected by plasma generation. The laser beam was absorbed by the plasma inside the groove, then laser fluence decreased to be close to the ablation threshold, which led to the formation of LIPSS.

3.3 Effect of Scanning Speed. Plane irradiation was performed at a pulse width of 50 ps, a laser fluence of 7.0 J/cm^2, and the laser was scanned five times with different scanning speeds. The SEM images of the irradiated surface at each scanning speed are shown in Fig. 6. The LIPSS formed at a scanning speed of 1.0 mm/s was more clear compared to that form at 10 mm/s. LIPSS formation might have been dependent on the overlap of laser pulses. The overlap increased with the decrease of the scanning speed, thus the interference between two adjacent laser irradiations became stronger. As a result, LIPSS formation became more significant. An AFM image and a cross-sectional profile of the LIPSS in Fig. 6(*a*) are shown in Figs. 7 and 8, respectively. The LIPSS have a period of about 300 nm and a depth of about 100 nm. Moreover, differently from the result of line irradiation, LIPSS could form on the surface even if the number of irradiations was 5. As the irradiation was performed at a scanning pitch of 2.0 μm, which was smaller than the spot diameter, the overlapped area was scanned more than the set number of irradiations, enabling LIPSS formation.

3.4 Mechanism of Laser-Induced Periodic Surface Structures Formation. In general, LIPSS are classified into two different types: LSFL and HSFL. LIPSS, which have a larger period than half of wavelength of laser beam, are called low-spatial frequency LIPSS (LSFL). On the other hand, LIPSS, which have a smaller period than half of laser wavelength, are called high-spatial frequency LIPSS (HSFL) [13,14]. It can be concluded that LIPSS generated in this study was HSFL because the period of generated LIPSS (300 nm) was smaller than half of laser wavelength (1030 nm). The mechanism of HSFL formation is still a controversial issue, which is under experimental and theoretical investigation. It was reported that the formation of LIPSS on zirconia surface in femtosecond laser irradiation is caused by the standing waves generated by the interference of the laser beam and the scattered wave [8]. It is expected that similar mechanism of LIPSS formation may take place in picosecond laser irradiation. Based on the results from this study, the possible mechanism of LIPSS formation on YSZ surface in picosecond laser irradiation is schematically shown in Fig. 9. When a laser beam strikes zirconia crystal which has a centrally asymmetric crystal structure (Fig. 9(*a*)), a high harmonic will be generated (Fig. 9(*b*)). The high harmonic interferes with the laser beam, then periodic asperities can form by ablation in the intensified area (Fig. 9(*c*)). In the area where ablation occurs, further ablation will be promoted by intensification of interference (Fig. 9(*d*)). As a result, periodic structure is formed by repeated irradiation.

3.5 Phase Transformation. Yttria-stabilized zirconia transforms from tetragonal to monoclinic due to thermal effect [4,15]. Since phase transformation causes strength reduction of YSZ, it is necessary to restrain phase transformation in laser processing. In this study, the peak intensities of the tetragonal and monoclinic phases were measured using a microlaser Raman spectrometer, and the results are shown in Fig. 10. A baseline was drawn in the figure to read the Raman peak intensity I. Then, the monoclinic ratio V_m was calculated from the Raman peak intensities using the following equation [16–19]:

$$V_m = \frac{I_m(181) + I_m(190)}{0.33 \times (I_t(151) + I_t(265)) + I_m(181) + I_m(190)} \quad (3)$$

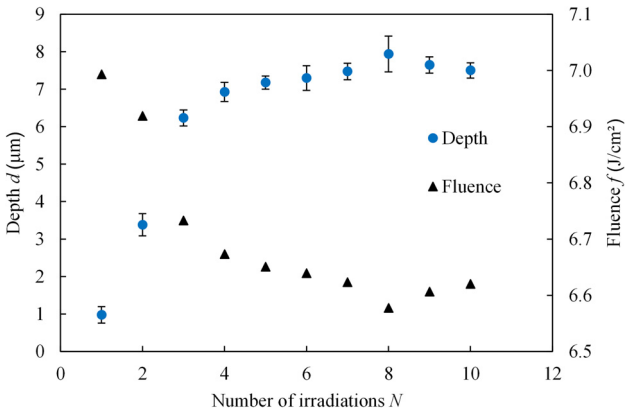

Fig. 5 Change in groove depth with number of irradiations

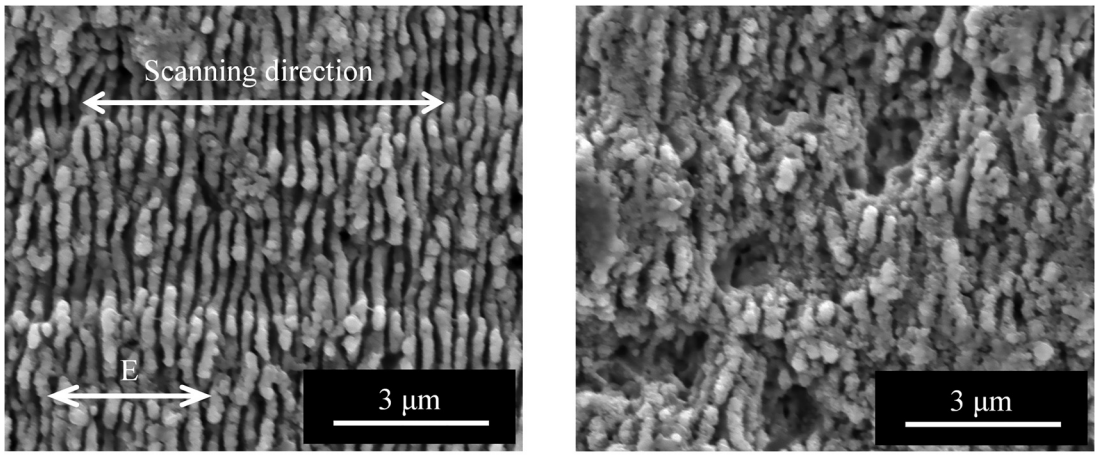

Fig. 6 SEM images of surface irradiated at various scanning speeds: (*a*) 1.0 mm/s and (*b*) 10 mm/s

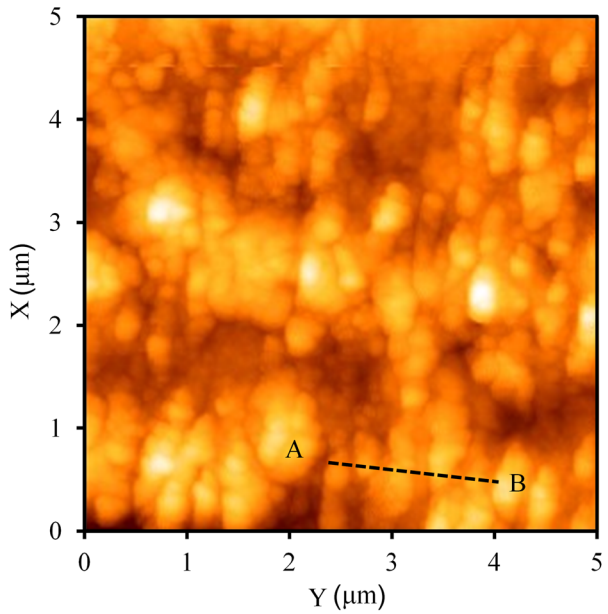

Fig. 7 AFM image of the LIPSS in Fig. 6(*a*)

where the subscripts m and t identify the monoclinic and tetragonal crystals, respectively. Using monoclinic ratio V_m we evaluated the phase transformation of YSZ after laser irradiation.

The monoclinic ratio for each condition is shown in Fig. 11. In this experiment, plane irradiation was performed at a pulse width of 50 ps and a scanning speed of 1.0 mm/s. Under this condition, LIPSS formation was confirmed on the surface when $N > 4$. In Fig. 11, it can be observed that the monoclinic ratio increases after irradiation and becomes the smallest at a laser fluence of 3.0 J/cm^2 when $N > 2$. In addition, at any laser fluence, the monoclinic ratio tends to decrease as the number of irradiations increases. It is presumable that the ablation depth becomes deeper by increasing the number of irradiations. Then the surface becomes out of the laser beam focus, and the laser fluence decreases. At a low laser fluence, the thermal effect is small and the ratio of phase transformation to monoclinic is also small. Therefore, the phase transformation can be restrained by reducing the laser fluence.

3.6 Surface Wettability. The contact angles of the sample surfaces before and after irradiation were measured using droplets of 5.0 μL pure water by a static sessile drop method. Figure 12 shows images of the water droplets on the unirradiated and the irradiated surface with LIPSS formation. To generate LIPSS on the surface, plane irradiation was performed at a pulse width of 50 ps, a laser fluence of 7.0 J/cm^2, a scanning speed of 1.0 mm/s, and the laser was scanned five times. As shown in Fig. 12, the contact angle was 76 deg for the unirradiated surface, but 27 deg after laser irradiation. The change of the contact angle with LIPSS formation is shown in Fig. 13. The water droplets spread evenly over

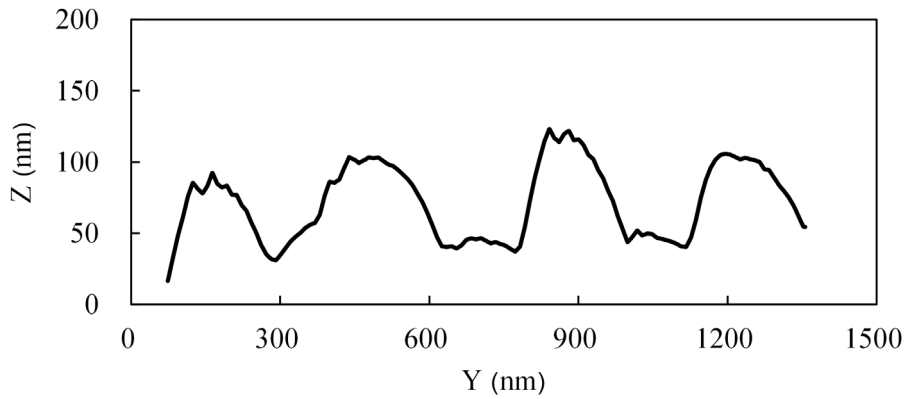

Fig. 8 Cross-sectional profile of the LIPSS in Fig. 6(*a*)

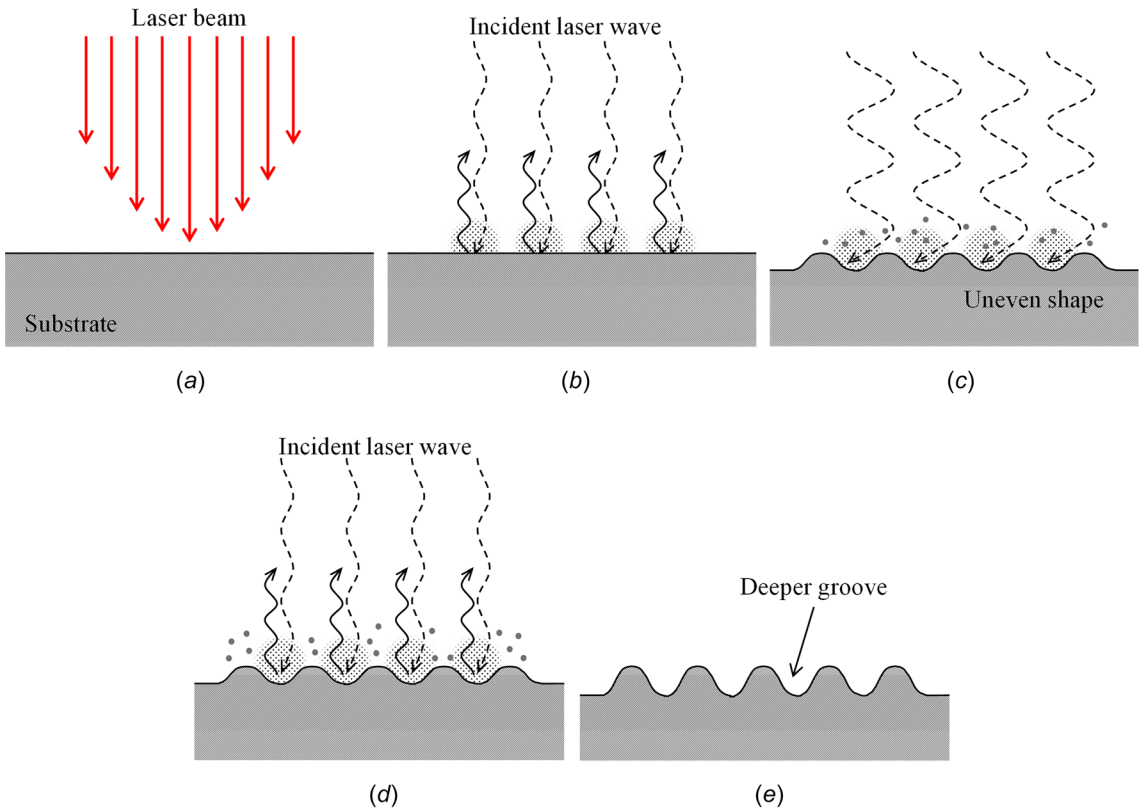

Fig. 9 Possible LIPSS formation mechanism on YSZ: (*a*) Laser irradiation, (*b*) high harmonic generation, (*c*) interference, (*d*) repetition, and (*e*) HSFL formation

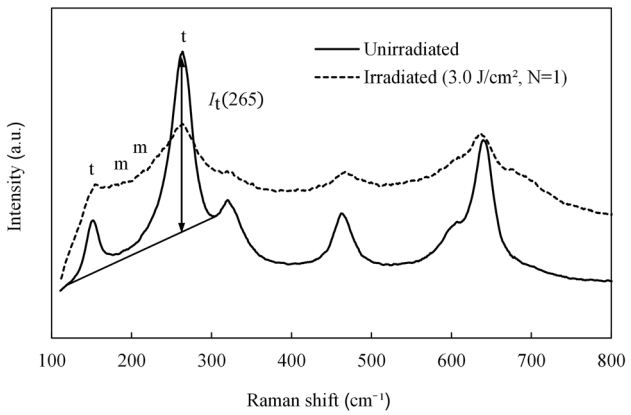

Fig. 10 Raman spectroscopy analysis of YSZ before/after laser irradiation

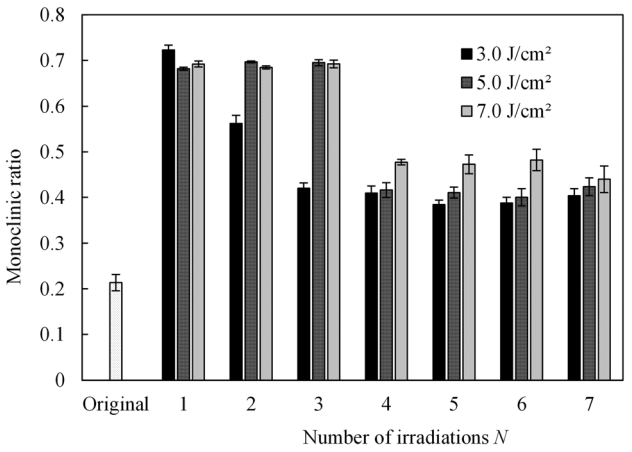

Fig. 11 Monoclinic ratio of irradiated surface under various irradiation conditions

the entire surface, and no dependence of contact angle on the periodic direction was observed.

Generally, surface wettability conditions can be classified into two states, Wenzel state and Cassie state [20,21]. When the Wenzel state dominates on the sample surface, liquid gets into the grooves and the contact area of liquid and sample surface increases. Therefore, the wettability of the original surface is enhanced. If the original surface was hydrophilic, it becomes more hydrophilic [20]. On the other hands, in the Cassie state, air is captured in the grooves, and the liquid–solid contact area becomes smaller. As a result, surface wettability shows hydrophobicity regardless of material original wettability [22,23]. In this study, the increase in hydrophilicity of YSZ after LIPSS formation may be attributed to the dominance of the Wenzel state.

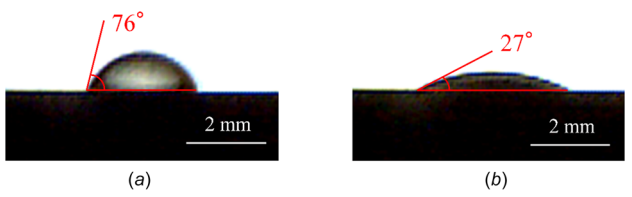

Fig. 12 Water droplets on unirradiated and irradiated surfaces: (*a*) unirradiated surface and (*b*) Irradiated surface (vertical direction)

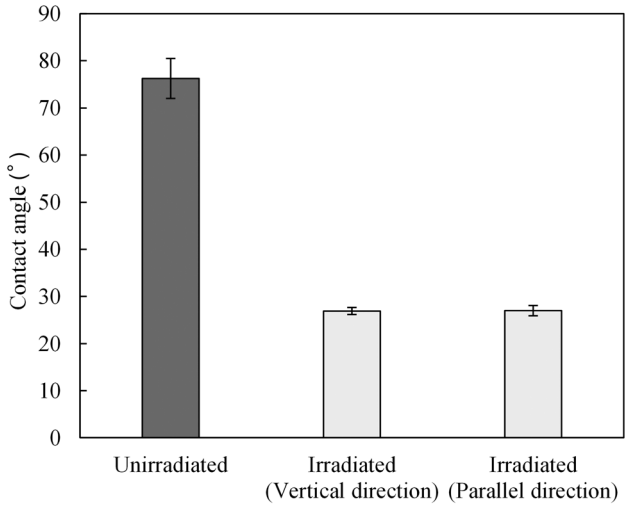

Fig. 13 Contact angle change of water droplets on unirradiated and irradiated surface

LIPSS formation increased the surface area of YSZ, improving the wettability of the surface.

4 Conclusions

Picosecond pulsed laser irradiation was performed on YSZ to investigate the fundamental microgrooving characteristics and conditions of LIPSS formation. The groove depth increased logarithmically with the increase of laser fluence. LIPSS, the period of which was about 300 nm, was successfully generated inside the microgrooves by increasing the number of irradiations. A lower scanning speed produced clearer LIPSS. LIPSS formed after less times of irradiation in plane irradiation compared with line irradiation due to laser spot overlap. Although phase transformation was observed after laser irradiation, it could be restrained by reducing the laser fluence or the number of irradiations. Furthermore, the formation of LIPSS on the YSZ surface greatly improved the surface hydrophilicity. This study showed the possibility of functionalization of YSZ surface with generating micro/nanoscale hybrid structure by picosecond pulsed laser irradiation.

References

[1] Scott, H. G., 1975, "Phase Relationships in the Zirconia-Yttria System," J. Mater. Sci., **10**(9), pp. 1527–1535.
[2] Gupta, T. K., Lange, F. F., and Bechtold, J. H., 1978, "Effect of Stress-Induced Phase Transformation on the Properties of Polycrystalline Zirconia Containing Metastable Tetragonal Phase," J. Mater. Sci., **13**(7), pp. 1464–1470.
[3] Sailer, I., Philipp, A., Zembic, A., Pjetursson, B. E., Hämmerle, C. H. F., and Zwahlen, M., 2009, "A Systematic Review of the Performance of Ceramic and Metal Implant Abutments Supporting Fixed Implant Reconstructions," Clin. Oral Implants Res., **20**(Suppl. 4), pp. 4–31.
[4] Li, J., Ji, L., Hu, Y., and Bao, Y., 2016, "Precise Micromachining of Yttria-Tetragonal Zirconia Polycrystal Ceramic Using 532 nm Nanosecond Laser," Ceram. Int., **42**(3), pp. 4377–4385.
[5] Wang, X., Shephard, J. D., Dear, F. C., and Hand, D. P., 2008, "Optimized Nanosecond Pulsed Laser Micromachining of Y-TZP Ceramics," J. Am. Ceram. Soc., **91**(2), pp. 391–397.
[6] Holthaus, M. G., Twardy, S., Stolle, J., Riemer, O., Treccani, L., Brinksmeier, E., and Rezwan, K., 2012, "Micromachining of Ceramic Surfaces: Hydroxyapatite and Zirconia," J. Mater. Process. Technol., **212**(3), pp. 614–624.
[7] Roitero, E., Anglada, M., Mücklich, F., and Jiménez-Piqué, E., 2018, "Mechanical Reliability of Dental Grade Zirconia After Laser Patterning," J. Mech. Behav. Biomed. Mater., **86**, pp. 257–263.
[8] Bashir, S., Rafique, M. S., and Husinsky, W., 2015, "Liquid Assisted Ablation of Zirconium for the Growth of LIPSS at Varying Pulse Durations and Pulse Energies by Femtosecond Laser Irradiation," Nucl. Instrum. Methods Phys. Res., Sect. B, **349**, pp. 230–238.
[9] Ali, N., Bashir, S., Umm-I-Kalsoom, M. S., Rafique, N., Begum, W., and Husinsky, W., 2017, "Nanostructuring of Zirconium by Femtosecond Laser Irradiation in the Ambient Environment of Air and Ethanol," Optik, **134**, pp. 149–160.
[10] KakehataYashiro, M., Oyane, H., Ito, A. A., and Torizuka, K., 2016, "Pulsewidth Dependence of Laser-Induced Periodic Surface Structure Formed on Yttria-Stabilized Zirconia Polycrystal," Proc. SPIE **9740**, p. 97401G.
[11] Salminen, T., Hahtala, M., Seppälä, I., Laukkanen, P., and Niemi, T., 2010, "Picosecond Pulse Laser Ablation of Yttria-Stabilized Zirconia From Kilohertz to Megahertz Repetition Rates," Appl. Phys. A: Mater. Sci. Process., **101**(4), pp. 735–738.
[12] Heiroth, S., Koch, J., Lippert, T., Wokaun, A., Günther, D., Garrelie, F., and Guillermin, M., 2010, "Laser Ablation Characteristics of Yttria-Doped Zirconia in the Nanosecond and Femtosecond Regimes," J. Appl. Phys., **107**(1), p. 014908.
[13] Bonse, J., Hohm, S., Kirner, S. V., Rosenfeld, A., and Kruger, J., 2017, "Laser-Induced Periodic Surface Structures-A Scientific Evergreen," IEEE J. Sel. Top. Quantum Electron., **23**(3), p. 9000615.
[14] Cahyadi, R. S., Torralva, B., and Yalisove, S. M., 2018, "High Spatial Frequency Periodic Structures Formation on Silicon Using Near UV Femtosecond Laser Irradiation," Appl. Phys. Lett., **112**(3), p. 032105.
[15] Piconi, C., and Maccauro, G., 1999, "Zirconia as a Ceramic Biomaterial," Biomaterials, **20**(1), pp. 1–25.
[16] Muñoz Tabares, J. A., and Anglada, M. J., 2010, "Quantitative Analysis of Monoclinic Phase in 3Y-TZP by Raman Spectroscopy," J. Am. Ceram. Soc., **93**(6), pp. 1790–1795.
[17] Pezzotti, G., and Porporati, A. A., 2004, "Raman Spectroscopic Analysis of Phase-Transformation and Stress Patterns in Zirconia Hip Joints," J. Biomed. Opt., **9**(2), p. 372.
[18] Kim, B. K., Hahn, J. W., and Han, K. R., 1997, "Quantitative Phase Analysis in Tetragonal-Rich Tetragonal/Monoclinic Two Phase Zirconia by Raman Spectroscopy," J. Mater. Sci. Lett., **16**(8), pp. 669–671.
[19] Roberts, O., Lunt, A., Ying, S., Sui, T., Baimpas, N., Dolbnya, I., Parkes, M., Dini, D., Kreynin, S., Neo, T., and Korsunsky, A., 2014, "A Study of Phase Transformation at the Surface of a Zirconia Ceramic," Lect. Notes Eng. Comput. Sci., **2**, pp. 1173–1177.
[20] Chen, F., Zhang, D., Yang, Q., Yong, J., Du, G., Si, J., Yun, F., and Hou, X., 2013, "Bioinspired Wetting Surface Via Laser Microfabrication," ACS Appl. Mater. Interfaces, **5**(15), pp. 6777–6792.
[21] Yao, L., and He, J., 2014, "Recent Progress in Antireflection and Self-Cleaning Technology—From Surface Engineering to Functional Surfaces," Prog. Mater. Sci., **61**, pp. 94–143.
[22] Long, J., Pan, L., Fan, P., Gong, D., Jiang, D., Zhang, H., Li, L., and Zhong, M., 2016, "Cassie-State Stability of Metallic Superhydrophobic Surfaces With Various Micro/Nanostructures Produced by a Femtosecond Laser," Langmuir, **32**(4), pp. 1065–1072.
[23] Dong, C., Gu, Y., Zhong, M., Li, L., Sezer, K., Ma, M., and Liu, W., 2011, "Fabrication of Superhydrophobic Cu Surfaces With Tunable Regular Micro and Random Nano-Scale Structures by Hybrid Laser Texture and Chemical Etching," J. Mater. Process. Technol., **211**(7), pp. 1234–1240.